CrystEngComm

Cite this: *CrystEngComm*, 2012, **14**, 1185

www.rsc.org/crystengcomm

COMMUNICATION

Facile synthesis of mesoporous CdS nanospheres and their application in photocatalytic degradation and adsorption of organic dyes†

Yuming Guo,* Jinfeng Wang, Zhikai Tao, Fangfang Dong, Kui Wang, Xiaoming Ma, Penghao Yang, Panpan Hu, Yiting Xu and Lin Yang*

Received 8th September 2011, Accepted 21st November 2011
DOI: 10.1039/c2ce06172d

CdS nanospheres with an average diameter of 40 nm, mesopores of 11.2 nm and a large specific surface area of 89.66 m^2 g^{-1} are fabricated successfully *via* a facile method under mild conditions. The as-prepared CdS nanospheres exhibit good performance in the photocatalytic degradation and adsorption activity for organic dyes.

As one of the most important II–VI semiconductors, CdS has a direct band gap of 2.42 eV and has been extensively investigated due to its unique physical and chemical properties. Nowadays, CdS is widely used in photoelectric conversion,[1–4] light-emitting diodes for flat-panel displays, lasers, thin film transistors, biological labeling, and other optical devices according to its excellent nonlinear properties.[5–10] Recently, CdS attracted tremendous attention for its new potential application as a nanoelectronic and photocatalytic material.[7,11–14] It is well-known that the properties and the corresponding applications of the CdS nanomaterials significantly depend on the size and architecture. Therefore, in recent years, a great deal of effort has been devoted to fabricate the CdS nanomaterials with a certain desired size and architecture through different methods. For example, CdS microspheres,[9] microflowers,[12] microdendrites,[15] nanotetrapods,[6] and microrods[16] have been prepared under hydrothermal or solvothermal conditions. In addition, CdS nanochains,[17] mesoporous tubular structures,[18] and bicrystalline CdS nanoribbons[19] have also been obtained. Although there have been significant achievements in the fabrication of the desired CdS nanomaterials, it is still a great challenge to develop a facile strategy to prepare the CdS nanomaterials, especially the mild and low-cost synthetic routes, which could greatly facilitate their future application in industry or scientific research. Moreover, to the best of our knowledge, the preparation and the potential application of the mesoporous CdS nanospheres have never been reported before.

Herein, a facile and rapid method is introduced to synthesize mesoporous PVP-modified CdS nanospheres (NSs) in the mixed solvent of EtOH/H_2O under mild conditions. In addition, the CdS NSs exhibit a unique optical property in the visible wavelength region. Moreover, the product can not only degrade the organic dyes rhodamine B (RhB) and methylene blue (MB) effectively under visible irradiation but also adsorb Congo red (CR) quickly in the dark.

In a typical experiment, $Cd(NO_3)_2 \cdot 4H_2O$ and PVP were dissolved into EtOH/H_2O mixed solvent (2 : 3, v/v) and stirred for 30 min under ambient conditions. Subsequently, TAA solution (100 mM) in ethanol/water mixed solvent was added quickly under moderate stirring, followed by dropping $NH_3 \cdot H_2O$ (1 : 1, v/v). Then, the reaction system was incubated at room temperature for 1 h. Afterward, the yellow products were centrifuged, washed with double distilled water (DD water) and absolute ethanol several times, and dried under vacuum at 40 °C for 8 h. For comparison, the control experiment was performed in the absence of PVP under identical conditions as the typical experiment.

From X-ray diffraction (XRD) analysis, the CdS NSs from the typical experiment exhibit identical diffraction peaks to the cubic phase CdS (JCPDF 42-1411), revealing the successful preparation of CdS (Fig. 1a). The diffraction peaks at 2θ of 27.55°, 44.68° and 53.03° can be indexed to (111), (220) and (311) planes of the cubic CdS, respectively. It should be noted that all the diffraction peaks are relatively broad, which can be attributed to the small size of the sample. In addition, the CdS Ctr from the control experiment exhibits an XRD pattern similar to the CdS NSs.

The size and morphology of the CdS NSs were determined using transmission electron microscopy (TEM) and scanning electron microscopy (SEM). The TEM image shown in Fig. 1b indicates that the CdS NSs exhibit spherical morphology and good dispersity. The size distribution analysis results in a narrow size distribution with the average diameter of 39.3 nm. The magnified TEM (inset of Fig. 1b) and FESEM images (Fig. 1c) show that the CdS NSs are composed of small nanoparticle building blocks with the average diameter of *ca.* 5 nm. Furthermore, the alternating pale and dark spots in each CdS nanosphere indicate the presence of pores between the building blocks. The HRTEM image in Fig. 1d shows that the CdS NSs present relatively good crystallinity. Meanwhile, the typical building blocks labeled by the white dotted line circles exhibit the fringe spacing of 0.3346 nm, 0.2042 nm, and 0.1734 nm, respectively, corresponding to the separation of (111), (220), and (311) planes. It reveals that the CdS NSs are polycrystalline, which is further confirmed by the corresponding diffused rings of the SAED pattern

College of Chemistry and Environmental Science, Key Laboratory of Green Chemical Media and Reactions, Ministry of Education, Henan Normal University, Xinxiang, 453007, P.R. China. E-mail: yanglin1819@163.com; guoyuming@gmail.com; Fax: +86-373-3328507; Tel: +86-373-3325058

† Electronic supplementary information (ESI) available. See DOI: 10.1039/c2ce06172d

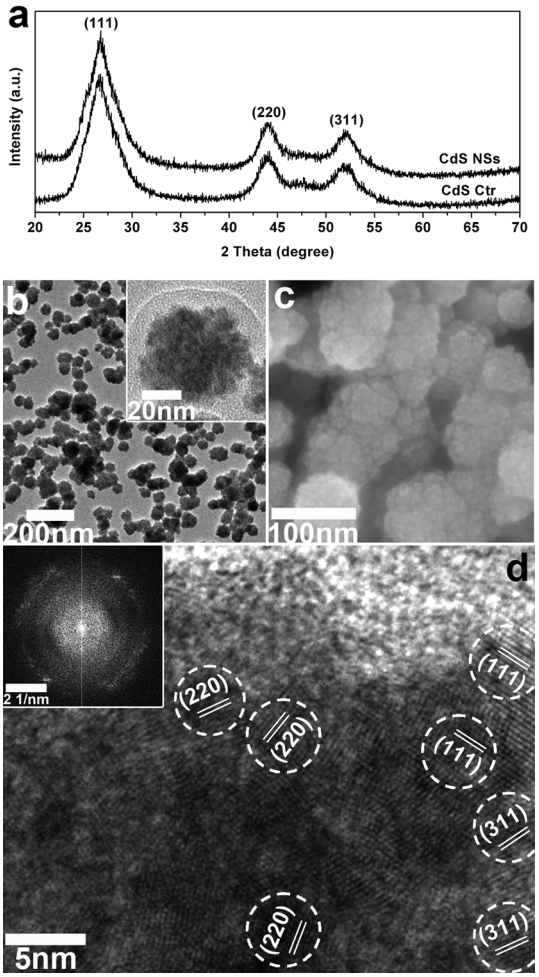

Fig. 1 (a) XRD pattern of the CdS NSs and CdS Ctr; (b) TEM image of the CdS NSs, inset: high magnified TEM image; (c) FESEM image of the CdS NSs; and (d) HRTEM image of the CdS NSs, inset: SAED pattern of the CdS NSs.

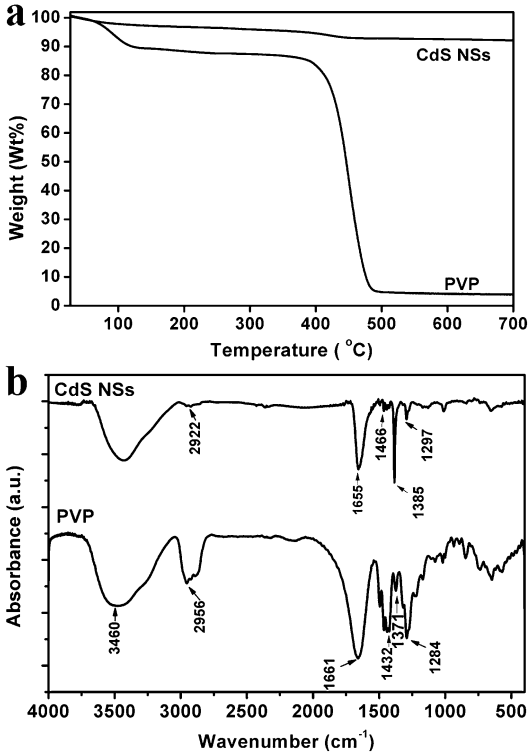

Fig. 2 (a) TGA curves of the pure PVP and CdS NSs. (b) FT-IR spectra of the pure PVP and CdS NSs.

(inset of Fig. 1d). In addition, SEM observations indicate the importance of PVP for the formation of the CdS NSs. The product from the control experiment performed in the absence of PVP exhibits serious agglomeration (Fig. S1a†). Whereas when PVP is introduced into the reaction system, the CdS NSs composed of nanoparticles can be prepared successfully (Fig. S1b†). These results reveal that PVP plays a crucial role in regulating the size, shape, dispersion and assembly behavior of CdS.

TGA analysis results reveal that the PVP content in the CdS NSs is about 5% (Fig. 2a). In Fig. 2a, comparing the TGA curve of the pure PVP, the mass loss of the as-prepared CdS NSs from 50 to 150 °C might be attributed to the evaporation of the absorbed moisture, whereas the mass loss of the CdS NSs (about 5%) in the second stage (150–475 °C) can be attributed to the thermal decomposition of the PVP.[20]

FT-IR measurements indicate the presence of PVP in the CdS NSs and the interactions between the CdS and the PVP. Comparing the spectrum of the CdS NSs with that of the PVP (Fig. 2b), the absorption bands of –C–H, $–CH_2$ from different areas of the PVP, and –C–N of the PVP molecules located at 2956, 1432, 1371, and 1284 cm^{-1} can be detected in the spectrum of the CdS NSs,[20,21] indicating the presence of PVP. Furthermore, the positions and intensities of these bands in the CdS NSs change to some extent, revealing the interaction between the CdS NSs and these groups. It is the presence of the PVP and these interactions that prevent the aggregation of the CdS NSs.

The specific surface area (SSA) and the porosity of the CdS NSs were determined using nitrogen adsorption/desorption analysis and the results are shown in Fig. 3a. According to the IUPAC classification, the obtained isotherm can be recognized as type IV, which is the typical characteristic of mesoporous materials.[22] In addition, the type H3 loop associated with slit-shaped pores occurs in the isotherm. As can be seen from the inset of Fig. 3a, the average pore size is 11.2 nm, indicating the mesoporous feature, which agrees well with the TEM and SEM observations. The multipoint Brunauer–Emmett–Teller (BET) analysis results in the large SSA for CdS NSs (89.66 $m^2 g^{-1}$), much larger than that of the CdS Ctr (19.46 $m^2 g^{-1}$). This suggests the more active reaction or adsorption sites accessible for the organic dyes.

The UV-vis and PL spectroscopy measurements showed the strong photoabsorption and photoluminescent properties of the CdS NSs. In the UV-vis spectrum (Fig. S2a†), the CdS NSs show a relatively broad absorption band from 200 to 600 nm, indicating the promising photoabsorption property in the visible light region. In the PL spectrum (Fig. S2b†), the CdS NSs exhibit a strong green emission near 511 nm at an excitation of 255 nm, which can be attributed to the recombination of the charge carriers within surface states.[23]

Photocatalytic activity evaluation results reveal that the as-prepared CdS NSs can effectively photocatalytically degrade the organic dyes including RhB and MB under visible light irradiation. From the results shown in Fig. 3b, after 120 min of irradiation, the

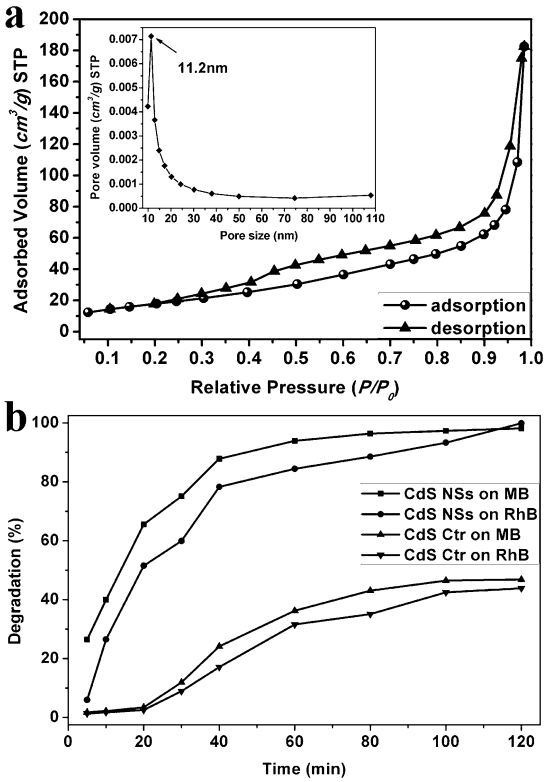

Fig. 3 (a) Nitrogen adsorption/desorption isotherm of the CdS NSs, inset: the corresponding BJH pore size distribution curve. (b) Photocatalytic degradation of RhB and MB in the presence of the CdS NSs and CdS Ctr under visible light irradiation.

photocatalytic degradation efficiency of the CdS NSs on RhB and MB can reach 97.44% and 98.15%, respectively, which are much higher than those of the CdS Ctr (46.84% and 43.87%). This excellent photodegradation performance of the CdS NSs can be attributed to their unique structural features, including the presence of the mesopores and the large SSA. The mesoporous architecture might enhance the opportunity for the organic dyes to penetrate into the inside of the CdS NSs and come in contact with the building blocks. The large SSA can afford the much more active sites accessible for the photodegradation reaction. Furthermore, the recycling result of the CdS NSs on the photocatalytic degradation of MB just showed a slight loss of the photocatalytic activity, revealing their excellent stability (Fig. S3†). The inductively coupled plasma-mass spectrometry (ICP-MS) analysis showed that there was only a trace amount of Cd^{2+} in the supernatant after 5 cycles of photocatalysis, confirming the long-term stability of the CdS NSs.

In addition to the application for the photocatalytic degradation of organic dyes, the potential application of the CdS NSs for the adsorption treatment of organic dyes is also evaluated. Fig. 4a presents the effect of the treatment time on the adsorption efficiency of CR with an initial concentration of 40 mg L^{-1} at room temperature. From the viewpoint of the economic issues, the treatment time required to reach equilibrium is important for the practical application of a certain adsorbent.[24] From the result, the adsorption rate is so fast that the equilibrium is achieved within 30 min, representing an advantage for water treatment system design.

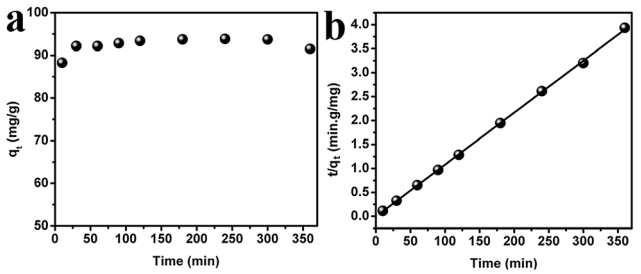

Fig. 4 (a) The adsorption curve of the CdS NSs on CR with different adsorption time. (b) Plot of pseudo-second-order kinetics.

In order to investigate the mechanism and kinetics of the adsorption, two well-known adsorption models, pseudo-first-order and pseudo-second-order equations,[25,26] were employed to explain the adsorption kinetics of the CdS NSs. The pseudo-first-order model is expressed as eqn (1):

$$\log (q_e - q_t) = \log q_e - \frac{k_1 t}{2.303} \quad (1)$$

where q_e and q_t are the amounts of CR adsorbed (mg L^{-1}) at equilibrium and time t (min), respectively. And k_1 (min^{-1}) is the pseudo-first-order adsorption rate constant. From the plot of pseudo-first-order kinetics for adsorption of CR onto CdS NSs shown in Fig. S4†, the R^2 value obtained is very small (0.0410), suggesting that the adsorption of CR onto CS NSs does not agree with the pseudo-first-order equation in our work.

The pseudo-second-order model is expressed as eqn (2):

$$\frac{t}{q_t} = \frac{1}{k_2 q_e^2} + \frac{t}{q_e} \quad (2)$$

where k_2 (g mg^{-1} min^{-1}) is the rate constant of pseudo-second-order adsorption. The linear plot of t/q_t *versus* t is shown in Fig. 4b and the obtained correlation coefficient R^2 value is very high (0.9997). This reveals good agreement with the pseudo-second-order model. Therefore, it is reasonable to describe the adsorption process of CR onto the CdS NSs with this model.

For a certain adsorbent, adsorption isotherms are used to determine the adsorption capacity of the adsorbent at different aqueous equilibrium concentrations and to study the adsorption mechanism between the adsorbent and the adsorbate. Fig. S5† depicts the equilibrium isotherm for CR on the CdS NSs. In the current study, Langmuir and Freundlich isotherm models are used to determine the maximum adsorption capacity of CdS NSs for CR. The Langmuir theory assumes that the adsorption occurs in a monolayer and there are no interactions among adsorbate molecules. The linear form of the Langmuir isotherm is expressed as eqn (3):[27]

$$\frac{C_e}{q_e} = \frac{1}{q_{max} K_L} + \frac{C_e}{q_{max}} \quad (3)$$

where C_e is the equilibrium concentration of CR in solution (mg L^{-1}), q_e is the equilibrium capacity of CR on the adsorbent (mg g^{-1}), q_{max} is the maximum adsorption capacity of the adsorbent corresponding and K_L is the Langmuir adsorption constant (L mg^{-1}) and is related to the free energy of adsorption. The plot of C_e/q_e *versus* C_e in Fig. 5a gives a straight line accompanied by a correlation coefficient R^2 of 0.9621 and a slope of 0.0041, indicating that the adsorption process does not obey the Langmuir adsorption isotherm so well. In addition,

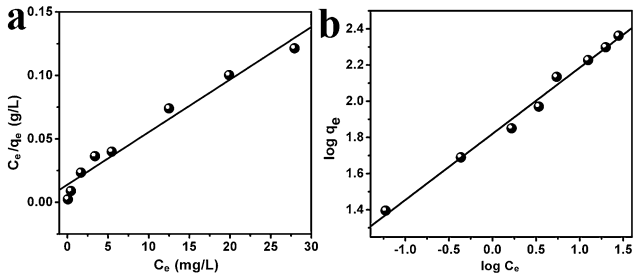

Fig. 5 Linear fitting results for CR adsorption onto the CdS NSs based on (a) Langmuir isotherm model and (b) Freundlich isotherm model.

from the slope of 0.0041, the q_{max} is calculated as 241.5 mg g^{-1}, which is far superior to the reported adsorption capacity.[28]

The Freundlich adsorption model assumes that adsorption occurs on heterogeneous surfaces. The Freundlich equation is an empirical equation and can be rearranged to a linear form as eqn (4):[29]

$$\log q_e = \log K_F + \frac{\log C_e}{n} \quad (4)$$

where q_e is the amount of dye adsorbed at equilibrium (mg g^{-1}), C_e is the equilibrium concentration remaining in the final solution (mg L^{-1}), K_F is the Freundlich constant (mg g^{-1})(L mg^{-1}) and $1/n$ is the heterogeneity factor describing the adsorption intensity. The result of log q_e against log C_e is presented in Fig. 5b, and the obtained correlation coefficient R^2 is 0.9891; the high R^2 indicated good agreement of the Freundlich isotherm with our adsorption cases. In addition, the value of n is 2.7 in terms of the slope; $n > 1$ predicts favorable adsorption activity of the CdS NSs.

To sum up, the mesoporous CdS NSs can be prepared successfully with the aid of PVP at room temperature. Based on the results, PVP plays a crucial role in the formation of the mesoporous CdS NSs. The synthetic strategy present here is facile, rapid, mild, and low-cost, and the target product can be fabricated with high throughput, which favors the scaled-up industrial applications and might shed new light on the synthesis of functional materials. In addition, the mesoporous CdS NSs exhibit excellent photocatalytic activity for the degradation of the organic dyes under visible light irradiation and efficient adsorption for Congo red. Hence, it is believed that the as-prepared mesoporous CdS NSs will find potential applications in the treatment of hazardous dyes through degradation or adsorption.

This work was financially supported by the National Science Foundation of China (21171051), the Program for Changjiang Scholars and Innovative Research Team in University (IRT1061), the Innovation Fund for Outstanding Scholar of Henan Province (114200510004), the Henan Key Proposed Program for Basic and Frontier Research (112102210005, 112300410095), the Natural Science Foundation of Henan Educational Committee (2010A150013) and the Henan Normal University College Students Innovation Experiment Program.

Notes and references

1 J. Bai, J. Li, Y. Liu, B. Zhou and W. Cai, *Appl. Catal., B*, 2010, **95**, 408–413.
2 X.-F. Gao, W.-T. Sun, Z.-D. Hu, G. Ai, Y.-L. Zhang, S. Feng, F. Li and L.-M. Peng, *J. Phys. Chem. C*, 2009, **113**, 20481–20485.
3 Y. R. Smith and V. Subramanian, *J. Phys. Chem. C*, 2011, **115**, 8376–8385.
4 S. C. Hayden, N. K. Allam and M. A. El-Sayed, *J. Am. Chem. Soc.*, 2010, **132**, 14406–14408.
5 C. J. Barrelet, Y. Wu, D. C. Bell and C. M. Lieber, *J. Am. Chem. Soc.*, 2003, **125**, 11498–11499.
6 J. E. Govan, E. Jan, A. Querejeta, N. A. Kotov and Y. K. Gun'ko, *Chem. Commun.*, 2010, **46**, 6072–6074.
7 S. K. Apte, S. N. Garaje, G. P. Mane, A. Vinu, S. D. Naik, D. P. Amalnerkar and B. B. Kale, *Small*, 2011, **7**, 957–964.
8 T. Zhai, X. Fang, Y. Bando, B. Dierre, B. Liu, H. Zeng, X. Xu, Y. Huang, X. Yuan, T. Sekiguchi and D. Golberg, *Adv. Funct. Mater.*, 2009, **19**, 2423–2430.
9 S. Rengaraj, S. Venkataraj, S. H. Jee, Y. Kim, C.-W. Tai, E. Repo, A. Koistinen, A. Ferancova and M. Sillanpää, *Langmuir*, 2011, **27**, 352–358.
10 T. Zhai, X. Fang, Y. Bando, Q. Liao, X. Xu, H. Zeng, Y. Ma, J. Yao and D. Golberg, *ACS Nano*, 2009, **3**, 949–959.
11 W. Fu, S. Qin, L. Liu, T.-H. Kim, S. Hellstrom, W. Wang, W. Liang, X. Bai, A.-P. Li and E. Wang, *Nano Lett.*, 2011, **11**, 1913–1918.
12 Y. Guo, J. Wang, L. Yang, J. Zhang, K. Jiang, W. Li, L. Wang and L. Jiang, *CrystEngComm*, 2011, **13**, 5045–5048.
13 Y. Guo, L. Wang, L. Yang, J. Zhang, L. Jiang and X. Ma, *Mater. Lett.*, 2011, **65**, 486–489.
14 S. Xiong, B. Xi and Y. Qian, *J. Phys. Chem. C*, 2010, **114**, 14029–14035.
15 D. Wang, D. Li, L. Guo, F. Fu, Z. Zhang and Q. Wei, *J. Phys. Chem. C*, 2009, **113**, 5984–5990.
16 F. Li, W. Bi, T. Kong, C. Wang, Z. Li and X. Huang, *J. Alloys Compd.*, 2009, **479**, 707–710.
17 C. Ge, M. Xu, J. Fang, J. Lei and H. Ju, *J. Phys. Chem. C*, 2008, **112**, 10602–10608.
18 W.-M. Zhang, N. Li, D.-H. Tang and Y.-Y. Wang, *Microporous Mesoporous Mater.*, 2011, **143**, 249–251.
19 X. Fan, M.-L. Zhang, I. Shafiq, W.-J. Zhang, C.-S. Lee and S.-T. Lee, *Cryst. Growth Des.*, 2009, **9**, 1375–1377.
20 Y. Cheng, B. Zou, C. Wang, Y. Liu, X. Fan, L. Zhu, Y. Wang, H. Ma and X. Cao, *CrystEngComm*, 2011, **13**, 2863–2870.
21 Y. Zhao, H. Wang, X. Lu, X. Li, Y. Yang and C. Wang, *Mater. Lett.*, 2008, **62**, 143–146.
22 K. S. W. Sing, D. H. Everett, R. A. W. Haul, L. Moscow, R. A. Pieroffl, J. Rouquerol and T. Siemieni-Ewska, *Pure Appl. Chem.*, 1985, **57**, 603–619.
23 H. Weller, *Angew. Chem., Int. Ed. Engl.*, 1993, **32**, 41–53.
24 L. Zhou, C. Gao and W. Xu, *ACS Appl. Mater. Interfaces*, 2010, **2**, 1483–1491.
25 I. A. W. Tan, A. L. Ahmad and B. H. Hameed, *J. Hazard. Mater.*, 2009, **164**, 473–482.
26 Y. S. Ho and G. McKay, *Chem. Eng. J.*, 1998, **70**, 115–124.
27 I. Langmuir, *J. Am. Chem. Soc.*, 1918, **40**, 1361–1403.
28 B. Cheng, Y. Le, W. Cai and J. Yu, *J. Hazard. Mater.*, 2011, **185**, 889–897.
29 H. M. F. Freundlich, *J. Phys. Chem. C*, 1906, **57**, 385–470.